DEFORMATION MICROSTRUCTURE OF A REDUCED-ACTIVATION FERRITIC/MARTENSITIC STEEL IRRADIATED IN HFIR - N. Hashimoto (Oak Ridge National Laboratory), M. Ando (Japan Atomic Energy Research Institute), H. Tanigawa (JAERI), T. Sawai (JAERI), K. Shiba (JAERI) and R.L. Klueh (ORNL)

OBJECTIVE

To determine the contributions of different microstructural features to strength and to deformation mode, transmission electron microscopy (TEM) specimens were prepared from the gage sections of the strained flat tensile specimens of irradiated F82H BM and its TIG weldments (weld metal and weld joint); fracture surfaces were examined by scanning electron microscopy (SEM).

SUMMARY

In order to determine the contributions of different microstructural features to strength and to deformation mode, the microstructures of deformed flat tensile specimens of irradiated reduced activation F82H (IEA heat) base metal (BM) and its tungsten inert-gas (TIG) weldments (weld metal and weld joint) were investigated by transmission electron microscopy (TEM), following fracture surface examination by scanning electron microscopy (SEM). After irradiation, the fracture surfaces of F82H BM and TIG weldment showed a martensitic mixed quasi-cleavage and ductile-dimple fracture. The microstructure of the deformed region of irradiated F82H BM contained dislocation channels. This suggests that dislocation channeling could be the dominant deformation mechanism in this steel, resulting in the loss of strain-hardening capacity. While, the necked region of the irradiated F82H TIG, which showed less hardening than F82H BM, showed deformation bands only. From these results, it is suggested that the pre-irradiation microstructure, especially the dislocation density, could affect the post-irradiation deformation mode.

PROGRESS AND STATUS

Introduction

For structural applications in fusion energy systems, ferritic/martensitic steels have several advantages based upon their resistance to void swelling, good thermal stress resistance, and well-established commercial production and fabrication technologies. Ferritic/martensitic steels, however, undergo radiation-induced hardening during neutron irradiation at temperatures up to 673-725K. Radiation hardening is often accompanied by a reduction in strain-hardening capacity and uniform elongation, and an increase in the temperature delineating the transition from quasi-cleavage to ductile fracture.

To investigate irradiation temperature dependence of hardening in ferritic/martensitic steels, F82H IEA base metal (BM) and its TIG weldments were irradiated in the High Flux Isotope Reactor (HFIR) of the Oak Ridge National Laboratory (ORNL). Irradiation conditions and further information on the experiment can be found elsewhere [1-4]. Stress-strain curves of F82H IEA base metal (BM) and the TIG weldment (TIG) irradiated at 573K and 773K in tests at RT are shown in figure 1(a) and (b), respectively [5,6]. In both F82H BM and TIG, the irradiation at 573K led to significant hardening and loss of strain-hardening capacity, while the specimens irradiated at 773K did not show irradiation hardening or degradation in ductility. The TIG specimen irradiated at 573K, however, showed a somewhat smaller irradiation hardening (e.g.; yield stress) compared to the BM specimen.

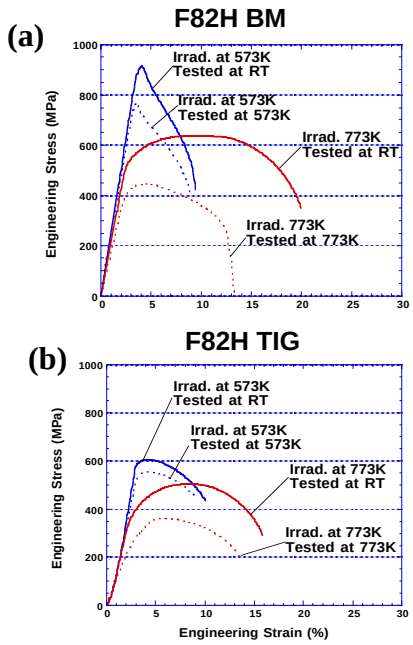

Fig. 1 Stress-strain curves of F82H BM (a) and TIG (b) irradiated at 573K and 773K in tests at RT

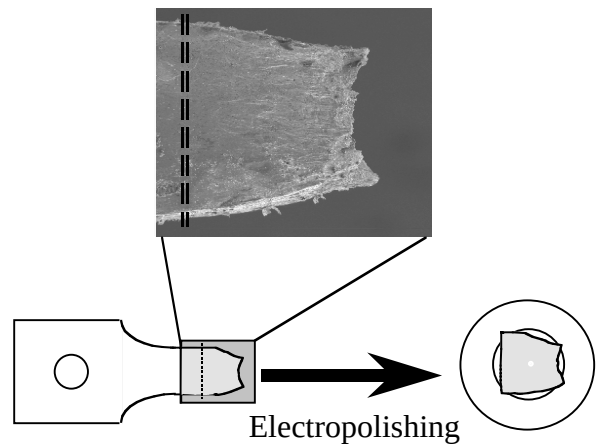

Fig. 2 Fabrication of TEM sample from the gauge section of F82H BM tensile specimen.

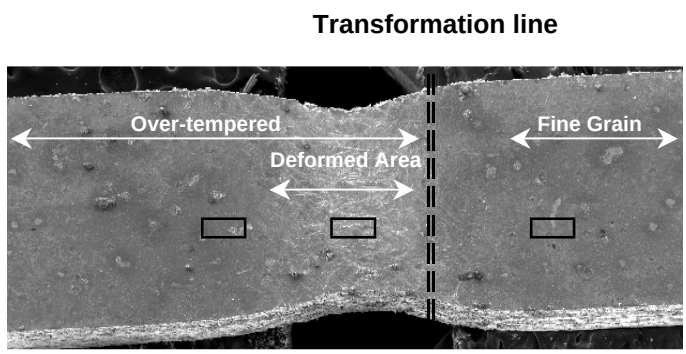

Fig. 3 TEM samples where taken from the over-tempered region, deformed area, and fine grain region of the deformed TIG specimen using FIB.

Experimental

The 8Cr-2WVTa steel F82H IEA was hot-rolled at 1473K and normalized at 1313K for 0.63 hrs followed by tempering at 1023K for 1 hr. TIG weldments were annealed at 993K for 1 hr. Chemical compositions of F82H IEA BM and TIG are given in the Ref.5. Neutron irradiation was performed up to 5 dpa at 573K and 773K in HFIR of ORNL. After post-irradiation tensile tests and SEM, TEM samples of BM and TIG were taken from the deformed specimen, followed by electropolishing (Fig.2) and fabrication using the Focused Ion Beam (FIB) (Fig.3) at Japan Atomic Energy Research Institute (JAERI). An FIB processor (Hitachi FB-2000A) with a microsampling system was used for ion machining and specimen manipulation. The fabrication with FIB has advantages of reducing ferromagnetism and radioactivity of irradiated ferritic steels. Further information on the FIB fabrication can be found in ref. 7.

A ferritic/martensitic steel weldment consists of weld metal, heat-affected zone (HAZ), and base metal. The HAZ is base metal that was affected by heating during welding, and the microstructural regions formed can be determined from the phase diagram. Immediately adjacent to the fusion line the base metal was heated to $T_{\gamma\delta}<T<T_m$, where $T_{\gamma\delta}$ is the temperature at which a two-phase region of austenite (γ) and δ-

ferrite begin to form on heating and T_m is the melting temperature. On cooling, the γ transforms to martensite. Next to this region is a region of base metal that transforms to γ on heating. The next region was heated to $A_{C1}<T<A_{C3}$ (A_{C1} is the temperature at which γ begins to form on heating), and it contains untempered martensite from the base metal that transformed to γ and over-tempered martensite. The remainder of the HAZ was heated to $T_T<T<A_{C1}$, where T_T is the tempering temperature of the base metal. This region contains over-tempered martensite.

Deformation and necking was shown (ref. 8) to occur in the over-tempered region immediately adjacent to the region where part of the microstructure transformed to austenite (Fig.3). TEM specimens were obtained from the deformed region and the over-tempered and transformed regions immediately adjacent to the deformed region.

Results and discussion

Fracture Surface

Fracture surfaces of F82H BM and TIG specimens irradiated at 573K and tested at RT at a strain rate of $1x10^{-3}$ s^{-1} are shown in Fig. 4. Fracture surfaces showed a typical martensitic mixed quasi-cleavage and ductile-dimple fracture in the center in both specimens. The sizes of large and small dimples were about 20-30mm and 10nm, respectively. The BM specimen seemed to include more large dimples than the TIG specimen.

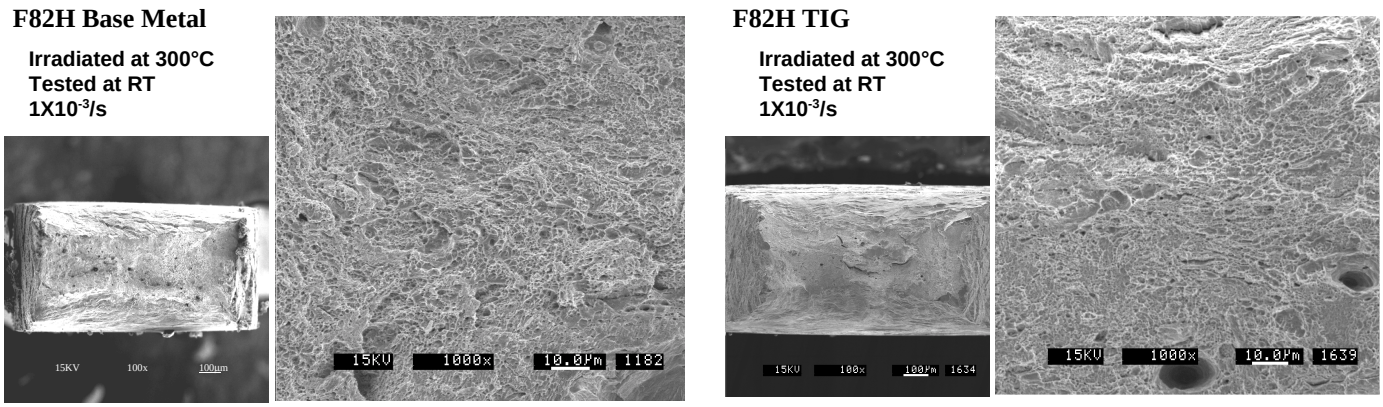

Fig. 4 Fracture surface of F82H base metal (BM) and TIG weldment specimens irradiated at 573K and tested at RT.

Microstructural Examination

Microstructure of Non-irradiated Specimens

Figure 5 shows microstructure of non-irradiated F82H BM, over-tempered region and fine grain region of TIG. The fine grain region showed finer grains than the BM and the over-tempered region. The BM and the fine grain region showed dislocations with a high density. Conversely, over-tempered region had a much lower dislocation density compared to the others.

Microstructure of As-irradiated Specimens

Figure 6 shows microstructure of the BM, the over-tempered region, and the fine grain region irradiated at 573K to 5 dpa in HFIR. In the BM, irradiation-induced dislocation loops were observed with a high number density. However, irradiation-induced precipitates and cavities were not observed.

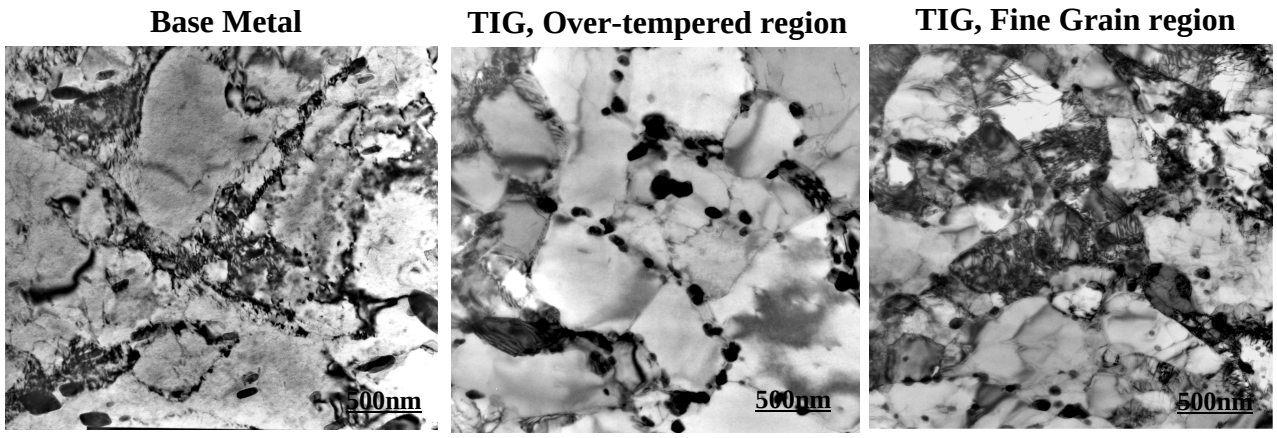

Fig. 5. Microstructure of non-irradiated F82H base metal., over-tempered region, and fine grain region of TIG weldment

Assuming the irradiation-induced obstacles to be dislocation loops only, the approximate value of α = 0.6, barrier strength of obstacles, was obtained for 573K, where a is defined by [9,10]

$$\alpha = \Delta\sigma_y / M\mu b(Nd)^{1/2}$$

where $\Delta\sigma_y$, M, b, N, d, and m are the increase in YS, the Tailor factor [11], the Burger's vector of dislocation, the number density of obstacles, the mean diameter of obstacles, and the shear modulus, respectively. Hardening contributions due to submicroscopic cavities or precipitates would reduce this calculated upper limit for the dislocation loop α.

On the other hand, the irradiated over-tempered and fine grain region showed no visible dislocation loops, while dislocation lines and helical dislocations decorated with defect clusters were observed, as seen in Fig.6. Furthermore, the number density of defect clusters in the TIG specimens was much smaller than in the BM. This could suggest that irradiation-introduced point defects such as vacancies and interstitials formed defect clusters along preexisting screw type dislocation lines and were absorbed by the screw dislocations.

Basically, there is no tensile and compressive stress field around a screw-type dislocation, but a shear stress is present, so that a screw-type dislocation is incapable of absorbing vacancies and interstitials. However, a screw-type dislocation could have a tensile and compressive stress field due to making edge components partially, and transform into helical dislocation by absorbing point defects. Therefore, the existence of a screw-type dislocations before irradiation could lead to a small number density of defect clusters and a lack of dislocation loops after irradiation, which would be barriers to moving dislocations during deformation. This is in good agreement with the tensile test results, showing that a lack of irradiation-induced dislocation loops led to a small yield stress increase (Fig.1).

Deformation Microstructure of Iirradiated Specimens

Figure 7 shows the microstructure of the deformed BM and TIG (over-tempered region) specimens irradiated at 573K to 5 dpa in HFIR. The microstructure in the necked region of the irradiated BM showed defect-free bands, indicative of dislocation channels (Fig.7(a)). The main deformation mode observed in the BM was dislocation channeling. The slip systems were identified as (110) $[\bar{1}11]$ and $(0\bar{1}1)$ [111], and the width and spacing of the channels was 100-120 nm and 480-520 nm, respectively. The moving dislocation sweeps the defects in the slip plane, leaving the slip plane depleted of them in its wake. Succeeding dislocations in the same plane will find fewer obstacles in their way, provoking a strong localization of the deformation in channel-like regions in the crystal. Gelles reported the deformed microstructure of irradiated Fe-9Cr uniaxial tensile specimens, showing elongated cavities in poorly defined narrow bands but no clear channels [12].

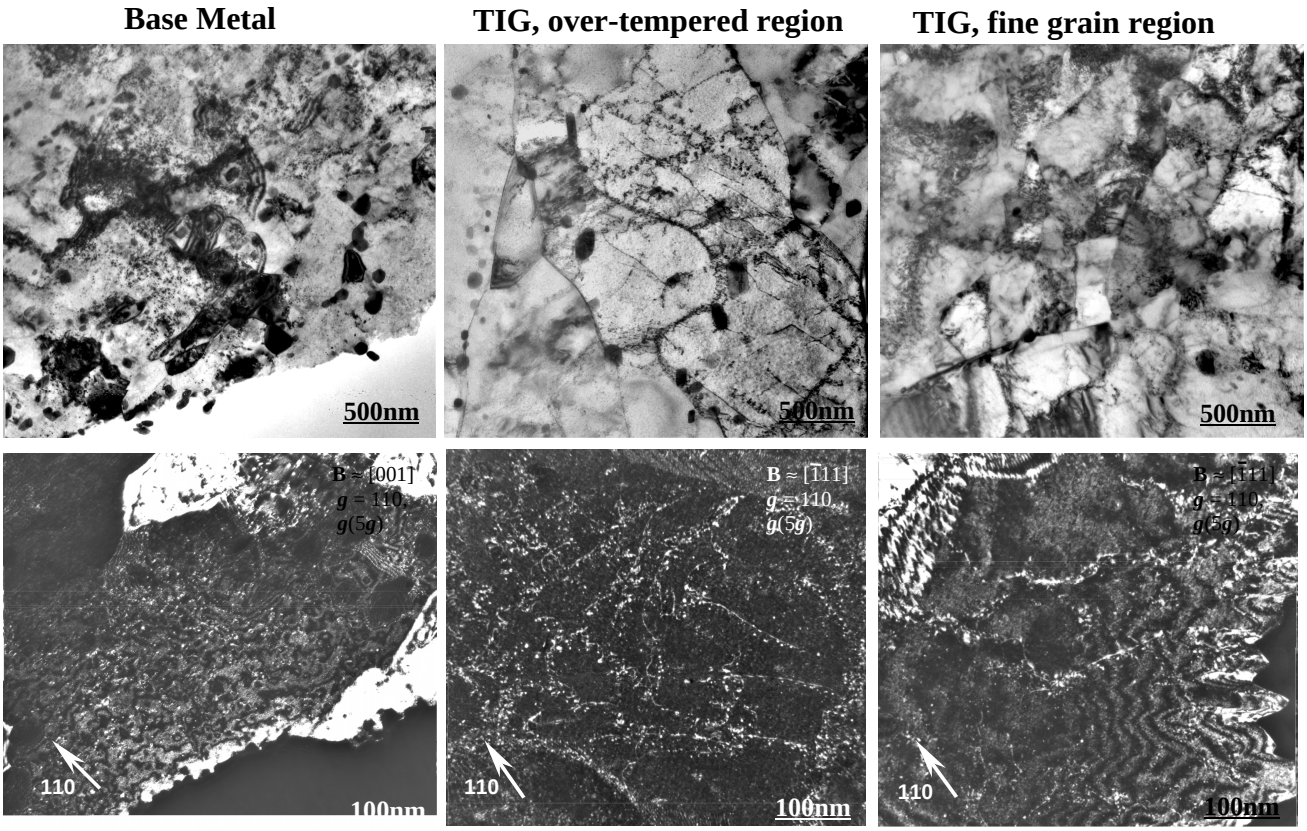

Fig. 6. Microstructure of irradiated F82H base metal, over-tempered region, and fine grain region of TIG weldment.

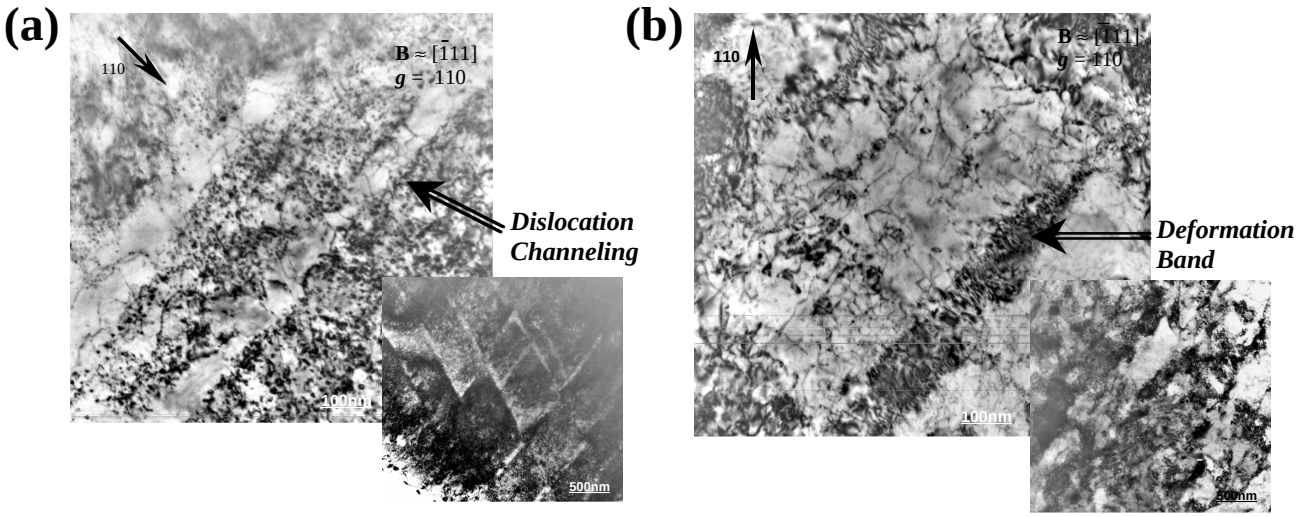

Slip plane: (110) and (0$\bar{1}$1)
Slip direction: [111] and [$\bar{1}$11]

Fig. 7. Microstructure of deformed F82H base metal (a) and over-tempered region of TIG weldment (b) irradiated at 573K to 5 dpa.

In contrast, the deformation microstructure of the irradiated TIG (over-tempered region) showed not dislocation channels but deformation bands (Fig.7(b)). Deformation bands with a 100 nm in width were lying on the (110). Since the irradiated TIG specimen had no dislocation loops and less defect clusters, dislocation channeling was not the dominant deformation mode.
These results suggest that the microstructure before irradiation could affect the development of secondary defects during irradiation, and also affect the dominant deformation mechanism.

Summary

In order to determine the contributions of different microstructural features to strength and to deformation mode, neutron-irradiated F82H (IEA heat) base metal and TIG weldments were investigated by transmission electron microscopy.

The microstructure of the deformed region of irradiated F82H BM showed dislocation channels, suggesting that dislocation channeling could be the dominant deformation mechanism in this steel, resulting in the loss of strain-hardening capacity. The necked region of irradiated F82H TIG (over-tempered region), which has less hardening than F82H BM, showed deformation bands. From these results, it is suggested that the pre-irradiation microstructure, especially one consisting of screw-type dislocations, could affect irradiation-induced secondary defect formation, leading to not only a lower yield stress but also a change in deformation mode after irradiation.

Acknowledgement

This research was sponsored by the Office of Fusion Energy Sciences, US Department of Energy under contract DE-AC05-96OR22464 with UT-Battelle, and the Japan Atomic Energy Research Institute.

REFERENCE

1) J.E. Pawel, K.E. Lenox, and I. Ioka, *Fusion materials semiannual progress report*, DOE/ER-0313/**19**, 312 (1995).
2) J.E. Pawel, K.E. Lenox, I. Ioka, and E. Wakai, *Fusion materials semiannual progress report*, DOE/ER-0313/**21**, 249 (1996).
3) M.L. Grossbeck, K.E. Lenox, M.A. Janney, T. Muroga, W.W. Heatherly, and K.R. Thoms, *Fusion materials semiannual progress report*, DOE/ER-0313/**22**, 254 (1997).
4) K.E. Lenox and M.L. Grossbeck, *Fusion materials semiannual progress report*, DOE/ER-0313/**25**, 307 (1998).
5) K. Shiba, R.L. Klueh, Y. Miwa, N. Igawa, and J.P. Robertson*, Fusion materials semiannual progress report*, DOE/ER-0313/**28**, 131 (2000).
6) N. Hashimoto, S.J. Zinkle, R.L Klueh, A.F. Rowcliffe, and K. Shiba, “Deformation Mechanisms in Martensitic Steels Irradiated in HFIR”, Microstructural Process in Irradiated Materials–2000, Mat. Res. Soc. Symp. Proc. Vol. **650** (2000) R1.10.
7) H. Tanigawa, M. Ando, Y. Katoh, T. Hirose, H. Sakasegawa, S. Jitsukawa, A. Kohyama, T. Iwai, J. Nucl. Mater. **297**, 279 (2001).
8) H. Tanigawa, N. Hashimoto, M. Ando, T. Sawai, K. Shiba, R.L. Klueh, in this proceedings
9) U.F. Kocks, *Metall. Trans.* **1**, 1121 (1970).
10) P.M. Kelly, *Int. Metal. Rev*. **18**, 31 (1973).
11) R.J. Asaro, Advances in *Applied Mechanics*, vol. **23**, Academic Press, New York, 1993, pp.1.
12) D.S. Gelles, R.E. Schäublin, *Mater. Sci. and Eng*. A **309-310**, 82 (2001).